Implementation of Pulse-width-Modulation Based Sliding Mode Controller for Boost Converters

Siew-Chong Tan, *Member, IEEE*, Y. M. Lai, *Member, IEEE*, and Chi K. Tse, *Fellow, IEEE*

***Abstract*—This letter addresses the various issues concerning the implementation of a pulse-width modulation (PWM) based sliding mode (SM) controller for boost converters. The methods of modeling the system and translation of the SM control equations for the PWM implementation are illustrated. It is shown that the control technique is easily realized with simple analog circuitries. Various experiments are conducted to test the static and dynamic performances of the system.**

***Index Terms*—Boost converter, sliding mode control, nonlinear controller, pulse-width modulation.**

I. Introduction

THE advantages of employing sliding mode (SM) controllers for applications in nonlinear control systems are well documented [1]. In power converters requiring wide operating range, SM controllers are understandably better candidates than conventional PWM controllers due to their excellent robust and stability properties in handling large-signal perturbations [2]. This has spurred much research in the area. However, among the various proposed systems, fixed-frequency SM controllers are particularly suited for practical implementation in power converters [3][4]–[10].

Study of fixed-frequency SM controllers has focused on the practical constraints of preventing excessive power losses and EMI noise generation and also on simplifying the design of input and output filters [11]. However, the nature of the SM controller is to operate ideally at infinite, varying, and self-oscillating switching frequencies such that the controlled variables can track a certain reference path to achieve steady-state operation [1].

Numerous methods have been proposed to constrict the switching frequency of SM controllers [3]–[10]. Those that employ hysteresis-modulation (HM) (or delta-modulation) as the medium for implementing the control law require either constant timer circuits to be incorporated into the hysteretic SM controller to ensure constant switching frequency [3], [4], or the use of an adaptive hysteresis band that varies with parameter changes to control and fix the switching frequency [5], [10]. However, these solutions require additional components and are unattractive for low-cost voltage conversion applications. Moreover, some of these converter systems suffer from a deteriorated transient response.

Alternatively, the switching frequency of SM controllers can be constricted (fixated) by changing the modulation method from HM to pulse width modulation (PWM) [2], [6], [7], [9]. This idea originated from one of the earliest papers on SM-controlled power converters [2], which suggests that under SM control, the control signal of the *equivalent control approach* $u_{\rm eq}$ in SM control is equivalent to the *duty cycle control signal* d of a PWM controller. The proof was later provided in another paper [12]. It has been shown that as the switching frequency tends to infinity, the averaged dynamics of an SM-controlled system is equivalent to the averaged dynamics of a PWM-controlled system, thus establishing the relationship $u_{\rm eq} = d$. Hence, the use of PWM techniques in lieu of HM methods in SM control is possible under these principles.

Lately, this idea has been revisited and experimentally demonstrated on a sliding-mode voltage-controlled (SMVC) buck converter [9]. Building on the work of [2], [6], [12], it is demonstrated in [9] how a PWM-based SM controller can be easily realized with simple analog ICs. However, the discussion does not cover the design methodology of other converters. It is also unknown if the proposed PWM-based SM controller can be as easily realized in more complex converters.

Therefore, in this letter, we extend the work in [9] by exploring the possible application of the PWM-based SM voltage controller on the boost converter. An overall description from modeling to the analog implementation of the system is provided. Experimental results are also provided to validate that the PWM-based SM controller under a different circuit architecture is also applicable to boost converters.

II. The Design Approach

A. System Modeling

A second-order PID type of SM voltage controller is adopted. Fig. 1 shows the schematic description of the proposed SMVC boost converters, where C, L, and $r_{\rm L}$ are the capacitance, inductance, and load resistance of the converters, respectively; i_C, i_L, and i_r are the capacitor, inductor, and load currents, respectively; $V_{\rm ref}, v_{\rm i}$, and $\beta v_{\rm o}$ are the reference, input, and sensed output voltage, respectively; and $u = 0$ or 1 is the switching state of power switch $S_{\rm W}$.

For any PID SMVC converter type, the control variable $\boldsymbol{x}$ may be expressed in the general form:

$$\boldsymbol{x} = \begin{bmatrix} x_1 \\ x_2 \\ x_3 \end{bmatrix} = \begin{bmatrix} V_{\rm ref} - \beta V_{\rm o} \\ \frac{d(V_{\rm ref} - \beta V_{\rm o})}{dt} \\ \int (V_{\rm ref} - \beta v_{\rm o}) dt \end{bmatrix} \quad (1)$$

Manuscript received May 19, 2005; revised December 7, 2005. This work was supported by a grant provided by The Hong Kong Polytechnic University (Project no. G-T379). Recommended by Associate Editor J. Sun.

The authors are with the Applied Nonlinear Circuits and Systems Research Group, Department of Electronic and Information Engineering, The Hong Kong Polytechnic University, Hung Hom, Kowloon, Hong Kong (e-mail: ensctan@eie.polyu.edu.hk).

Digital Object Identifier 10.1109/LPEL.2005.863269

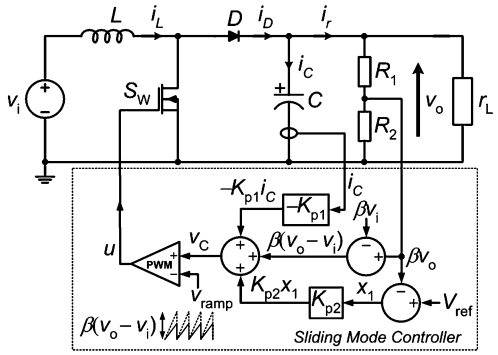

Fig. 1. Schematic diagrams of the PID SMVC boost converter.

where x_1, x_2, and x_3 represent the *voltage error*, the *voltage error dynamics* (or the rate of change of voltage error), and the *integral of voltage error*, respectively. Substitution of the boost converter's behavioral models under continuous conduction mode (CCM) of operation into (1) produces the following control variable description:

$$\boldsymbol{x}_{\text{boost}} = \begin{bmatrix} V_{\text{ref}} - \beta v_{\text{o}} \\ \frac{\beta v_{\text{o}}}{r_{\text{L}}C} + \int \frac{\beta(v_{\text{o}} - v_{\text{i}})\bar{u}}{LC} dt \\ \int x_1 dt \end{bmatrix} \tag{2}$$

where $\bar{u} = 1 - u$ is the inverse logic of u. Next, the time differentiation of (2) produces the state-space description

$$\dot{\boldsymbol{x}}_{\text{boost}} = \mathbf{A}\boldsymbol{x}_{\text{boost}} + \mathbf{B}\bar{u} \tag{3}$$

where

$$\mathbf{A} = \begin{bmatrix} 0 & 1 & 0 \\ 0 & -\frac{1}{r_{\text{L}}C} & 0 \\ 1 & 0 & 0 \end{bmatrix} \quad \text{and} \quad \mathbf{B} = \begin{bmatrix} 0 \\ \frac{\beta v_{\text{o}}}{LC} - \frac{\beta v_{\text{i}}}{LC} \\ 0 \end{bmatrix}. \tag{4}$$

B. Controller Design

For this system, it is appropriate to have a general SM control law that adopts a switching function such as

$$u = \begin{cases} 1 & \text{when } S > 0 \\ 0 & \text{when } S < 0 \end{cases} \tag{5}$$

where S is the instantaneous state variable's trajectory and is described as

$$S = \alpha_1 x_1 + \alpha_2 x_2 + \alpha_3 x_3 = \boldsymbol{J}^{\text{T}}\boldsymbol{x}, \tag{6}$$

with $\boldsymbol{J}^{\text{T}} = [\alpha_1 \ \alpha_2 \ \alpha_3]$ and α_1, α_2, and α_3 representing the control parameters termed as sliding coefficients.

1) Derivation of Existence Conditions: To ensure the existence[1] of the SM operation, the local reachability condition

$$\lim_{S \to 0} S \cdot \dot{S} < 0 \tag{7}$$

[1]Satisfaction of the existence condition is one of the three necessary conditions for SM control operation to occur. It ensures that the state trajectory at locations near the sliding surface will always be directed toward the sliding surface. The other two necessary conditions are the hitting condition, which is satisfied by the control law in (5), and the stability condition, which is satisfied through the assignment of sliding coefficients [13].

TABLE I
BOOST CONVERTER SPECIFICATIONS

Description	Parameter	Nominal Value
Input voltage	v_{i}	24 V
Capacitance	C	2000 μF
Capacitor ESR	c_r	69 mΩ
Inductance	L	300 μH
Inductor resistance	l_r	0.14 Ω
Switching frequency	f_{S}	200 kHz
Minimum load resistance (full load)	$r_{\text{L(min)}}$	24 Ω
Maximum load resistance (10 % load)	$r_{\text{L(max)}}$	240 Ω
Desired output voltage	V_{od}	48 V

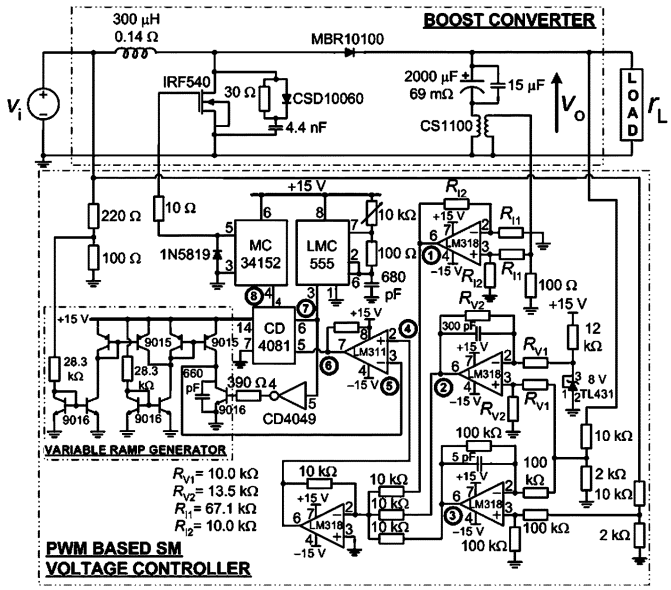

Fig. 2. Schematic diagram of the proposed PWM-based SMVC boost converter.

TABLE II
THEORETICAL DESCRIPTION OF SIGNALS

Test Location	Description
1	$\beta L\left(\frac{\alpha_1}{\alpha_2} - \frac{1}{r_{\text{L}}C}\right) i_C$
2	$-LC\frac{\alpha_3}{\alpha_2}\left(V_{\text{ref}} - \beta v_{\text{o}}\right)$
3	$-\beta\left(v_{\text{o}} - v_{\text{i}}\right)$
4	v_{c}
5	$\hat{v}_{\text{ramp}}$
6	u_{PWM}
7	u_{CLK}
8	$u = u_{\text{PWM}} \bullet u_{\text{CLK}}$

must be satisfied. For the proposed converter, this can be expressed as

$$\begin{cases} \dot{S}_{S\to 0^+} = \boldsymbol{J}^{\text{T}}\mathbf{A}\boldsymbol{x}_{\text{boost}} + \boldsymbol{J}^{\text{T}}\mathbf{B}u_{S\to 0^+} < 0 \\ \dot{S}_{S\to 0^-} = \boldsymbol{J}^{\text{T}}\mathbf{A}\boldsymbol{x}_{\text{boost}} + \boldsymbol{J}^{\text{T}}\mathbf{B}u_{S\to 0^-} > 0. \end{cases} \tag{8}$$

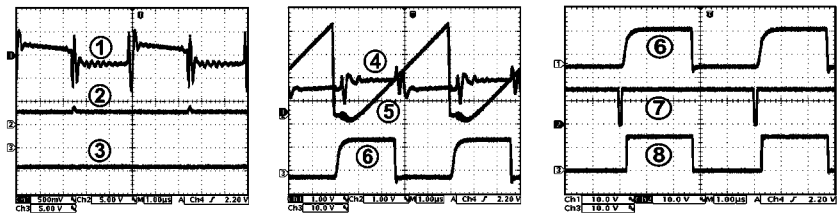

Fig. 3. Experimental waveforms of the test locations under full-load operation.

TABLE III
LOAD REGULATION PROPERTY: OUTPUT VOLTAGE AT NOMINAL OPERATING CONDITION $v_{\rm i} = 24$ V AND $r_{\rm L} = 24\ \Omega$ IS $v_{\rm o(nominal\ condition)} = 47.95$ V

Input Voltage	Voltage Deviation: $\Delta v_{\rm o} = v_{\rm o(240\ \Omega)} - v_{\rm o(24\ \Omega)}$	Percentage Change: $\frac{\Delta v_{\rm o}}{v_{\rm o(nominal\ condition)}}$ x 100 %
$v_{\rm i}$= 20 V	0.84 V	1.75 % of $v_{\rm o(nominal\ condition)}$
$v_{\rm i}$= 24 V	0.61 V	1.27 % of $v_{\rm o(nominal\ condition)}$
$v_{\rm i}$= 28 V	0.56 V	1.16 % of $v_{\rm o(nominal\ condition)}$

TABLE IV
LINE REGULATION PROPERTY: OUTPUT VOLTAGE AT NOMINAL OPERATING CONDITION $v_{\rm i} = 24$ V AND $r_{\rm L} = 24\ \Omega$ IS $v_{\rm o}({\rm nominal\ condition}) = 47.95$ V

Loading Condition	Voltage Deviation: $\Delta v_{\rm o} = v_{\rm o(v_i=20\ V)} - v_{\rm o(v_i=28\ V)}$	Percentage Change: $\frac{\Delta v_{\rm o}}{v_{\rm o(nominal\ condition)}}$ x 100 %
Minimum load (240 Ω)	0.68 V	1.42 % of $v_{\rm o(nominal\ condition)}$
Half load (48 Ω)	0.58 V	1.21 % of $v_{\rm o(nominal\ condition)}$
Full load (24 Ω)	0.40 V	0.83 % of $v_{\rm o(nominal\ condition)}$

The specific conditions for the existence of the SM control operation for boost converters are as follows.

- Case 1: $S \to 0^+, \dot{S} < 0$—substitution of $u_{S\to 0^+} = \bar{u} = 0$, and the matrices in (2) and (4) into (8) gives $-\alpha_1(\beta i_C)/(C) + \alpha_2(\beta i_C)/(r_{\rm L}C^2) + \alpha_3(V_{\rm ref} - \beta v_{\rm o}) < 0$.
- Case 2: $S \to 0^-, \dot{S} > 0-$ substitution of $u_{S\to 0-} = \bar{u} = 1$, and the matrices in (2) and (4) into (8) gives $-\alpha_1(\beta i_C)/(C) + \alpha_2(\beta i_C)/(r_{\rm L}C^2) + \alpha_3(V_{\rm ref} - \beta v_{\rm o}) - \alpha_2(\beta v_{\rm i})/(LC) + \alpha_2(\beta v_{\rm o})/(LC) > 0$.

Finally, the combination of both inequalities gives the simplified existence condition

$$0 < \beta L\left(\frac{\alpha_1}{\alpha_2} - \frac{1}{r_{\rm L}C}\right) i_C - LC\frac{\alpha_3}{\alpha_2}\left(V_{\rm ref} - \beta v_{\rm o}\right) < \beta(v_{\rm o} - v_{\rm i}). \quad (9)$$

2) Derivation of Control Equations for the PWM-Based Controller: The conventional SM controller implementation based on HM [8] requires only control equations (5) and (6). However, if the PWM-based SM voltage controller is to be adopted, an indirect translation of the SM control law is required so that PWM can be used in lieu of hysteresis modulation [9]. The procedure for the PWM design can be summarized in two steps. Firstly, the equivalent control signal $u_{\rm eq}$, which is a smooth function of the discrete input function u, is formulated using the *invariance conditions* by setting the time differentiation of (6) as $\dot{S} = 0$ [1]. Secondly, the equivalent control function is mapped onto the duty cycle function of the pulse-width modulator [9]. For the PWM-based SMVC boost converter, the derivations are as illustrated.

- Equating $\dot{S} = \boldsymbol{J}^{\rm T}\mathbf{A}\boldsymbol{x} + \boldsymbol{J}^{\rm T}\mathbf{B}\bar{u}_{\rm eq} = 0$ yields the equivalent control function

$$\bar{u}_{\rm eq} = -\left[\boldsymbol{J}^{\rm T}\mathbf{B}\right]^{-1}\boldsymbol{J}^{\rm T}\mathbf{A}\boldsymbol{x} = \frac{\beta L}{\beta(v_{\rm o} - v_{\rm i})} \times \left(\frac{\alpha_1}{\alpha_2} - \frac{1}{r_{\rm L}C}\right) i_C - \frac{\alpha_3 LC}{\alpha_2\beta(v_{\rm o} - v_{\rm i})}(V_{\rm ref} - \beta v_{\rm o}) \quad (10)$$

where $\bar{u}_{\rm eq}$ is continuous and $0 < \bar{u}_{\rm eq} < 1$. Since $u = 1 - \bar{u}$, which also implies $u_{\rm eq} = 1 - \bar{u}_{\rm eq}$, the substitution of (10) into the inequality gives

$$0 < u_{\rm eq} = 1 - \left[\frac{\beta L}{\beta\left(v_{\rm o} - v_{\rm i}\right)}\left(\frac{\alpha_1}{\alpha_2} - \frac{1}{r_L C}\right) i_C - \frac{\alpha_3 LC}{\alpha_2\beta(v_{\rm o} - v_{\rm i})}(V_{\rm ref} - \beta v_{\rm o})\right] < 1. \quad (11)$$

Multiplication of the inequality by $\beta(v_{\rm o} - v_{\rm i})$ gives

$$0 < {u_{\rm eq}}^* = -\beta L\left(\frac{\alpha_1}{\alpha_2} - \frac{1}{r_{\rm L}C}\right) i_C + LC\frac{\alpha_3}{\alpha_2}(V_{\rm ref} - \beta v_{\rm o}) + \beta(v_{\rm o} - v_{\rm i}) < \beta(v_{\rm o} - v_{\rm i}). \quad (12)$$

- Finally, the mapping of the equivalent control function (12) onto the duty ratio control d, where $0 < d =$

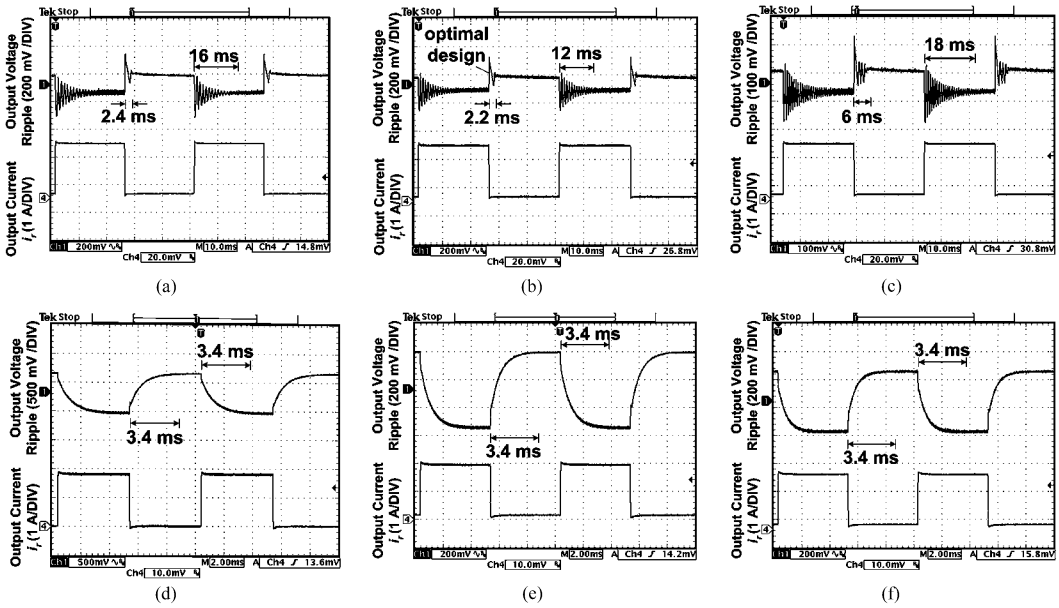

Fig. 4. Experimental waveforms of output voltage ripple $\widetilde{v_{\rm o}}$ and output current i_r of the boost converter, with the peak current mode controller (a)–(c) and the 1.5 krad/s bandwidth PWM based SM controller (d)–(f), operating at load resistance alternating at 24 Ω (minimum) and 240 Ω (maximum).

$(v_{\rm c})/)(\hat{v}_{\rm ramp}) < 1$, gives the following relationships for the control signal $v_{\rm c}$ and ramp signal $\hat{v}_{\rm ramp}$ where

$$v_{\rm c} = u_{\rm eq}{}^{*} = -\beta L\left(\frac{\alpha_1}{\alpha_2} - \frac{1}{r_{\rm L}C}\right) i_C + LC\frac{\alpha_3}{\alpha_2}(V_{\rm ref} - \beta v_{\rm o}) + \beta(v_{\rm o} - v_{\rm i}) \tag{13}$$

and

$$\hat{v}_{\rm ramp} = \beta(v_{\rm o} - v_{\rm i}) \tag{14}$$

for the practical implementation of the PWM-based SM controller.

III. Implementation of the PWM-Based SM Controller

A. Conversion of Control Equations to Circuit Form

1) Control Signal Computation: The computation of the control signal $v_{\rm c}$ in (13) can be performed using simple gain amplification and summing functions. In our prototype, we realize the equation using only three analog gain amplifiers and a summer circuit (LM318). The parameters of these circuitries can be easily calculated using known values of $L, C, r_{\rm L}$, and β, and proper choices of α_1, α_2, and α_3.

2) Ramp Signal Generation: The peak magnitude of the variable ramp signal $\hat{v}_{\rm ramp}$ is to follow description (14). In our prototype, a transistor configuration of multiple current mirror circuitries (9015 and 9016) and a charging capacitor are employed to realize the ramp generation. Since the desired output voltage is normally constant with little deviation, only the input voltage change is considered in the design. As for the frequency of the ramp signal, it is controlled by an impulse generator (LMC555 and CD4049).

3) Duty Cycle Protection: The incorporation of the control and ramp signal circuitries into the pulse-width modulator (LM311) forms the basic architecture of the PWM-based SM controller. However, recalling that the boost type converter cannot operate with a switching signal u that has a duty cycle $d = 1$, a small protective circuitry is required to ensure that the duty cycle of the controller's output is always $d < 1$. In our prototype, this is satisfied by multiplying the logic state $u_{\rm PWM}$ of the pulse-width modulator with the logic state $u_{\rm CLK}$ of the impulse generator using a logic AND IC chip (CD4081). By doing so, the maximum duty cycle of the controller is clamped by the duty cycle of the impulse generator.

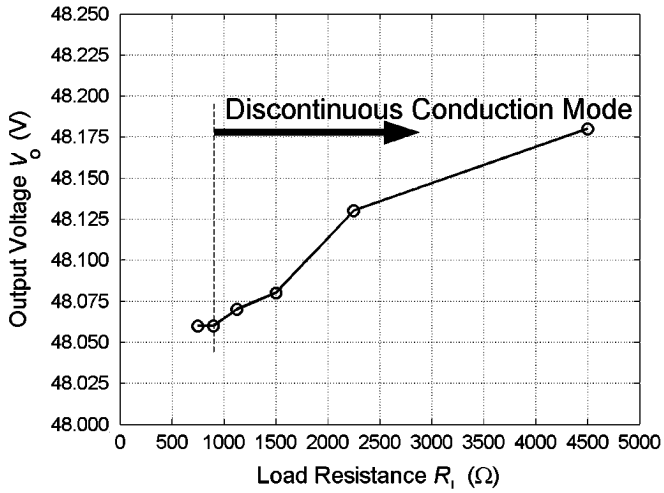

Fig. 5. Graphs of dc output voltage $v_{\rm o}$ against load resistance $R_{\rm L}$ for the PWM-based SMVC boost converter in light load conditions.

4) Switching Frequency Selection: The adoption of fixed frequency transforms the SM controller into a type of quasi sliding-mode controller, which operates as an approximation of the ideal SM controller. The consequence of this transformation is the reduction of the system's robustness and the deterioration of the regulation properties. Similar to all other types of controller, the performance of this controller improves with a higher switching frequency. Likewise, the selection of

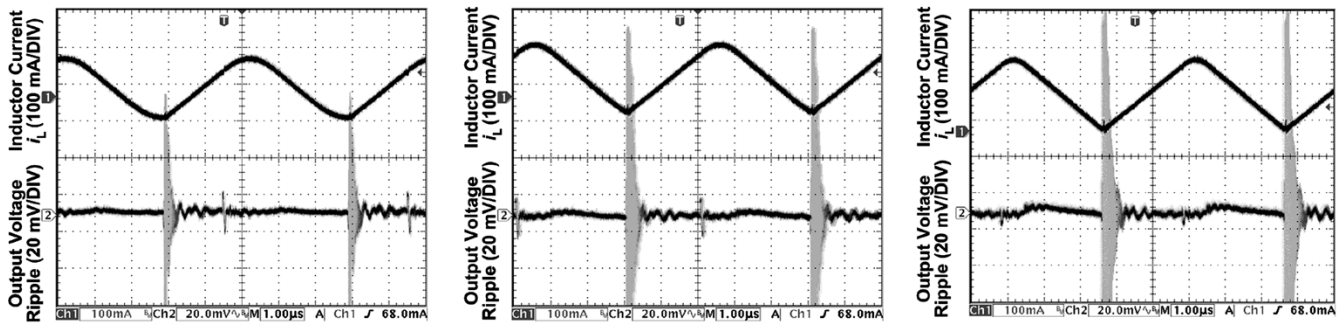

Fig. 6. Waveforms of inductor current i_L and output voltage ripple $\widetilde{v_o}$ of the PWM-based SMVC boost converter operating in discontinuous conduction mode with (a) no operating load; (b) 10 mA load current; and (c) 30 mA load current.

the switching frequency should be a balance between control performance and the converter's specifications.

B. Experimental Prototype

The derived controller is verified through an experimental prototype developed with the specifications shown in Table I.

Fig. 2 shows the schematic diagram of the proposed PWM-based SMVC boost converter. The enumerated points on the diagram represent different test locations in the controller where waveforms are captured and analyzed. The theoretical description of the signals is derived and shown in Table II.

IV. Experimental Results and Discussions

A. Measured Signal of Test Locations

Fig. 3 shows the steady-state waveforms of the test locations when the converter is operating at full-load. The captured results are consistent with theoretical expectations.

B. Steady-State Performance

A tabulation of the data in terms of the load and line regulation properties is also given in Tables III and IV, respectively. According to Table III, the maximum load-regulation error occurs at $v_{\rm i} = 20$ V, with a deviation of 1.75% from $v_{\rm o(nominal\ condition)}$. Similarly, it can be found from Table IV that the maximum line-regulation error occurs at minimum load $r_{\rm L} = 240\ \Omega$, with a deviation of 1.42% from $v_{\rm o(nominal\ condition)}$.

C. Transient Performance

The dynamic behavior of the proposed PWM controller is compared to that of a UC3843 PWM peak-current-mode controller that is optimally tuned to operate a boost converter at a step-load change from $R_{\rm L} = 24\ \Omega$ to $R_{\rm L} = 240\ \Omega$ for the input condition $V_{\rm i} = 24$ V. Fig. 4(a)–(f) show the experimental waveforms of the boost converter under these control schemes.

It can be seen that with the PWM peak-current-mode controller, the dynamic behavior of the system differs for different operating conditions. Specifically, the response becomes more oscillatory at higher input voltages. Moreover, the dynamic behavior and transient settling time are also very much different between the cases when the load changes from $R_{\rm L} = 24\ \Omega$ and $R_{\rm L} = 240\ \Omega$ and when it changes from $R_{\rm L} = 240\ \Omega$ and $R_{\rm L} = 24\ \Omega$. This is expected since the peak-current-mode controller is designed under a linearized small-signal model that is only optimal for a specific operating condition. Thus, when a different operating condition is engaged, the response varies.

On the other hand, with the PWM-based SM voltage controller, the dynamic behavior of the output voltage ripple is basically similar (i.e., critically damped) for all operating input and load conditions. Moreover, the transient setting time, which is around 3.4 ms, is also independent of the direction of the step-load change. This demonstrates the strength of the SM controller in terms of robustness in the dynamic behavior under different operating conditions and uncertainties. Additionally, the example also illustrates a major difference between a large-signal controlled system (SM) and a small-signal controlled system (PWM), that is, the former complies with the design giving a similar response for all operating conditions, while the response of the latter will only comply with the design at a specific operating condition.

D. Operating in Discontinuous Conduction Mode

The PWM-based SMVC boost converter, which is designed for operation in CCM, is also tested in discontinuous conduction mode (DCM). Fig. 5 shows the variation of the dc output voltage against different operating load resistances in the DCM. The voltage regulation of the converter has a 0.12 V deviation (i.e., 0.25% of $V_{\rm od}$) in $v_{\rm o}$ for the DCM load range $900\ \Omega \leq r_{\rm L} \leq 4500\ \Omega$, i.e., load regulation $(dv_{\rm o})/(dr_{\rm L})$ averages at 0.033mV/Ω. Fig. 6(a), (b), and (c) show, respectively, the behavior of the inductor current and the output voltage ripple at DCM when the converter is operating at no load, 10 mA, and 30 mA currents. It can be concluded from the results that the converter is applicable to light-load operations in the DCM.

V. Conclusion

The implementation of a fixed-frequency PWM-based SM voltage controller for a boost converter is presented in this letter. It is shown that the control technique is easily realized with simple analog circuitries. Various experiments are conducted to test the static and dynamic performances of the system. It can be concluded that the derived controller/converter system is feasible for common step-up conversion purposes.

ACKNOWLEDGMENT

The authors would like to acknowledge Y. L. Cheng and C. K. Wu for their contributions in constructing the experimental prototype.

REFERENCES

[1] V. Utkin, J. Guldner, and J. X. Shi, *Sliding Mode Control in Electromechanical Systems*, London, U.K.: Taylor & Francis, 1999.

[2] R. Venkataramanan, A. Sabanoivc, and S. Čuk, "Sliding mode control of DC-to-DC converters," in *Proc. IEEE Conf. Industrial Electronics, Control and Instrumentations (IECON)*, 1985, pp. 251–258.

[3] B. J. Cardoso, A. F. Moreira, B. R. Menezes, and P. C. Cortizo, "Analysis of switching frequency reduction methods applied to sliding mode controlled dc-dc converters," in *Proc. IEEE Applied Power Electronics Conf. Expo. (APEC)*, 1992, pp. 403–410.

[4] P. Mattavelli, L. Rossetto, G. Spiazzi, and P. Tenti, "General-purpose sliding-mode controller for dc/dc converter applications," in *IEEE Power Electronics Specialists Conf. Rec. (PESC)*, 1993, pp. 609–615.

[5] V. M. Nguyen and C. Q. Lee, "Tracking control of buck converter using sliding-mode with adaptive hysteresis," in *IEEE Power Electronics Specialists Conf. Rec. (PESC)*, 1995, pp. 1086–1093.

[6] ——, "Indirect implementations of sliding-mode control law in buck-type converters," in *Proc. IEEE Applied Power Electronics Conf. and Expo. (APEC)*, 1996, pp. 111–115.

[7] S. K. Mazumder and S. L. Kamisetty, "Experimental validation of a novel multiphase nonlinear VRM controller," in *IEEE Power Electronics Specialists Conf. Rec. (PESC)*, 2004, pp. 2114–2120.

[8] S.-C. Tan, Y. M. Lai, M. K. H. Cheung, and C. K. Tse, "On the practical design of a sliding mode voltage controlled buck converter," *IEEE Trans. Power Electron.*, vol. 20, no. 2, pp. 425–437, Mar. 2005.

[9] S. C. Tan, Y. M. Lai, C. K. Tse, and M. K. H. Cheung, "A fixed-frequency pulse-width-modulation based quasisliding mode controller for buck converters," *IEEE Trans. Power Electron.*, vol. 20, no. 6, pp. 1379–1392, Nov. 2005.

[10] S. C. Tan, Y. M. Lai, and C. K. Tse, "Adaptive feedforward and feedback control schemes for sliding mode controlled power converters," *IEEE Trans. Power Electron.*, vol. 21, no. 1, pp. 182–192, Jan. 2006.

[11] H. W. Whittington, B. W. Flynn, and D. E. Macpherson, *Switched Mode Power Supplies: Design and Construction*, 2nd ed. New York: Wiley, 1997.

[12] H. Sira-Ramirez, "A geometric approach to pulse-width modulated control in nolinear dynamical systems," *IEEE Trans. Automat. Contr.*, vol. 34, no. 3, pp. 184–187, Feb. 1989.

[13] J. Ackermann and V. Utkin, "Sliding mode control design based on Ackermann's formula," *IEEE Trans. Automat. Contr.*, vol. 43, no. 2, pp. 234–237, Feb. 1998.